Project Number: 774571
Start Date of Project: 2017/11/01
Duration: 48 months

Type of document 4.4 – V1.0

Drought Stress Detection

Dissemination level	PU
Submission Date	2020-11-15
Work Package	WP4
Task	T4:6
Type	Report
Version	1.0
Author	Mario Gilcher, Steve Ahlswede, Cristian Silvestri, Marco Paolocci
Approved by	Andrea Gasparri, Valerio Cristofori, Emanuele Garone, PMC

Executive Summary

This document describes the details of the data acquisition (see section 2) and pre-processing (see section 3) of *Task 4.6 Water Stress Measurement* as well as the analysis steps towards UAV based drought stress detection algorithms. As a final result, drought stress related indices are presented (see section 4.3) and used to model the on-site relative water content (RWC) and necrotic leaf area (NLA) of the plants (see section 4.5). We were able to show, that all relevant indices could be computed with the current setup, and the orthomosaics could be preprocessed and tightly integrated into the database system (see section 5.2). Limitations of the modeling approach, as shown by our validation, can be explained by inconsistencies in the data acquisition caused by administrative restrictions and COVID-19 logistical difficulties, as well as a lack of drought stress effects on the field (see section 5.1) that limited the validation of the method. In conclusion, a robust processing chain was established, all causes for possible technical problems in the data acquisition were identified, and clear guidelines to optimize our results in 2021 were developed (see section 5.3).

Table of Contents

Abbreviations and Acronyms

CWSI	Crop Water Stress Index
DEM	Digital Elevation model
DN	Digital Number
GPS	Global Positioning Systems
I	Irrigated
NDVI	Normalized Difference Vegetation Index
NI	Non-Irrigated
NLA	Necrotic Leaf Area
PRI	Photochemical Reflectance Index
RGB	Red-Green-Blue
RWC	Relative Water Content
Simple Ratio	SR
UAV	Unmanned Aerial Vehicle

List of Figures

List of Tables

1 Introduction

The aim of this task is to detect possible water stress within a hazelnut orchard, as well as to differentiate water stress from disease infections, using multispectral remote sensing in the visible to near infrared (VNIR) range and thermal data by the means of unmanned aerial vehicles (UAV). The multispectral and thermal data is analyzed and used to predict the current state of the phenology in regards to leaf water content (RWC) and spread of diseases (NLA).

As a first step, we describe our data acquisition process, with a focus on the UAV campaign, which is supplemented with field data collected on the ground. Afterwards, we describe the preprocessing steps of orthomosaicking, georeferencing, harmonizing the acquired imagery, as well as present the resulting indices. We then describe the relationship between the aerial imagery and the ground truth data with linear models, the result of which we apply to produce spatially explicit maps of RWC and NLA.

In a last step we discuss these results by investigating the limiting factors we encountered while validating these models. We give a clear summary of all the issues we encountered, what we did to improve the data quality this year, and an overview of the actions foreseen for next year to maximize the quality of the data.

2 Data collection campaign 2020

2.1 Experimental set-up

For water stress detection, 10 adult trees and 10 young trees located in PANTHEON's fields 18 and 16, respectively, were selected (Figure 1). Field 18 is characterized by adult trees planted in a 5.0m x 5.0m layout, whereas field 16 is characterized by young trees planted in a 4.5m x 3.0m layout.

An underground irrigation drip line between each planting row allowed us to control which rows received irrigation over the course of the experiment. Thus, one row from each field was placed into the irrigation group (I), and the other into the non-irrigation group (NI).

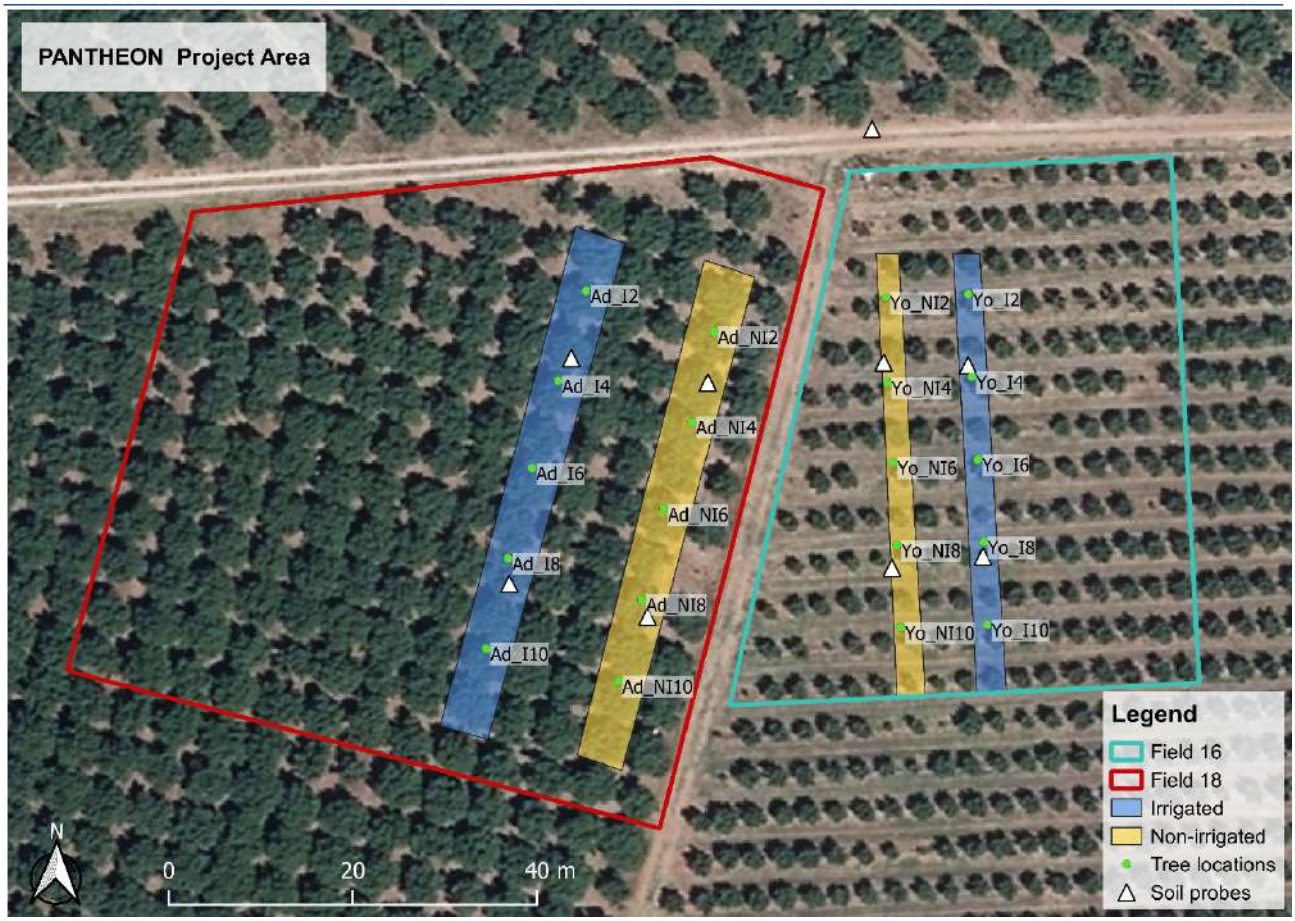

Figure 1 - Overview of the experimental setup for the water stress experiments. Tree locations are labeled with the tree's identifier.

The irrigation experiment was performed from July 2, 2020 until August 22, 2020. Field 16 had an irrigation schedule of three days per week (Wednesday, Thursday, Saturday), receiving 215m^3 water per day. Field 18 received irrigation five days a week (Monday – Friday), receiving 405m^3 water per day.

Diseases were also monitored for the same 20 trees. Diseases were allowed to spread uncontrolled in the area, with ground truth measurements being taken five times during the 2020 season.

2.2 Data collection overview

Ground truth data for tree disease and water stress were collected from the beginning of July until the beginning of September, while UAV campaigns spanned from July 12th until September 20th (Figure 2). A total of 20 trees were investigated; five young non-irrigated trees, five young irrigated trees, five adult non-irrigated trees, and five adult irrigated trees. Figure 1 shows the positions of each tree in the field.

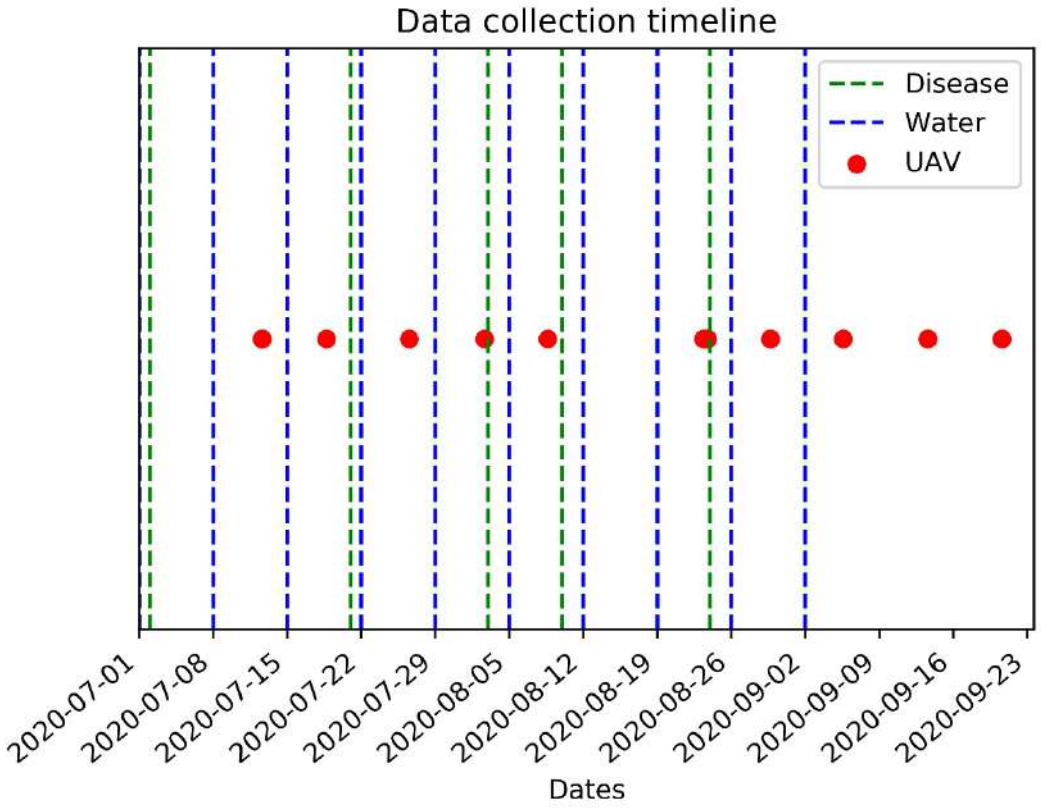

Figure 2 - Timeline of the data collection dates for the 2020 season. Disease measurements related to necrotic leaf area are shown in green, water measurements of relative leaf water content are shown in blue, and UAV flights are in red.

2.3 UAV data

Three cameras were mounted on the UAV: an RGB camera (Sony α5100), a customized six-band multi-spectral camera (Tetracam MCAW-6), and a thermal camera (TeAx ThermalCapture-2.0) (Table 1). For the collection of UAV imagery, the drone was flown at an altitude of about 30 meters for the first month of data collection. However, due to a change of status of a nearby airfield, flight altitudes were suddenly limited to 25 m from August onwards. The UAV was flown at a speed of about 1 meter per second.

Band Name	Center Wavelength (nm)	Bandwidth FWHM (nm)
Sony α5100		
Blue	~400-530	~100
Green	~460-630	~100
Red	~570-700	~130
Tetracam MCAW-6		
Green	530.7	3
Green-Yellow	550.0	10
Yellow-Green	570.0	10
Red	680.0	10
Red-Edge	720.0	10
Near-infrared	900.0	10
TeAx ThermalCapture 2.0		
Thermal	7.5-13.5 µm	N/A

Table 1 - Sensors mounted on the UAV.

UAV missions were planned ahead of the 2020 season such that flights were performed within a few days of ground truth data collection dates.

It must be remarked that given the legislative uncertainty and the COVID situation the mission planning and execution faced a number of logistic problems. A first source of uncertainty was based on the ambiguity regarding the set of rules we had to comply with. Initially it was expected that the more lenient European Union Aviation Safety Agency (EASA) flight rules would have come into effect from the 1st of July 2020. However, due to COVID, the adoption of these rules has been postponed to 2021.

Even more important than this, our mission planning faced two difficulties linked to the specific location where our orchard is located:

1) The area in which the orchard is located is inside a flight military zone marked as a Romeo Area. The rules of this specific area allow flights only during a short time span every week (from Saturday 13:00 to Sunday midnight).

2) In the middle of the summer, the status of a recreational aviation airfield a few kilometers away from the orchard changed, suddenly limiting the flying altitude on the orchard to 25 meters.

Each of these problems plays a role in the quality of the collected data. Firstly, being restricted to flights from Saturday afternoon until Sunday introduced logistical difficulties, such as having to wait an entire week before we could collect data again. This meant that weekend flights with sub-optimal field conditions could not be shifted to a weekday, nor could flights be easily repeated given the discovery of a system failure. In order to mitigate these issues, we planned missions on a near weekly basis. In addition, two flights per day were scheduled, allowing us to obtain a large amount of data and to compensate for possible holes in the data

collection due for example to sensor failures. Given that this problem was known before the 2020 campaign, a request of exception for the summer 2020 was also submitted to the military aviation authorities but remained unanswered.

The 25m limitation on the maximum flight altitude appeared suddenly at the halfway point of the data collection campaign of 2020, at which point all sensors and mission plans had been calibrated for a higher altitude. Unfortunately, accordingly to our flight regulation experts, the process to request an exception to fly at higher altitude takes a minimum of 40 days, and therefore there was no way to solve this problem for the remainder of the 2020 campaign. Accordingly, we had to recalibrate the missions and the sensors for the new altitude. A height of 25 meters is far from ideal as the quality of the images become very dependent to exposure and focus issues. Additionally, the size of the study fields was too large to cover a in a single flight, leading to a loss in our ability to collect extra data to guard against holes in the data collection.

Last but not least, it is worth to mention that the strict lockdown in Italy and associated travel difficulties did not allow the pre-season week of testing and tuning of the drone and camera. Instead we were forced to test and tune the drone during the data acquisition campaign which (due to travel restrictions) was mostly performed via remote communication with the pilot.

In the end, a total of ten flight days were performed during this season (Table 3), with two flights per day on each day except for August 23rd, where a total of 8 flights were carried out over the course of the day (refer to section 3.3 for more details).

2.4 Ground truth data collection

In order to quantify water stress and disease, ground truth data was collected for RWC and NLA, respectively.

2.4.1 Water stress

Relative water content is a measure of plant water status in terms of the physiological consequence of cellular water deficit [1]. It estimates the current water content of the sampled leaf tissue relative to the maximal water content it can hold at full turgidity. Normal values of RWC range between 98% in fully turgid transpiring leaves to about 30-40% in severely desiccated and dying leaves, depending on plant species. In most crop species the typical leaf RWC at around initial wilting is about 60% to 70%, with exceptions [1]. The RWC was measured for all young and adult plants subjected to irrigated and non-irrigated water regimes. RWC was determined in fully expanded leaves collected in well-developed vegetative shoots selected at half-crown height. Two leaves per plant were collected, one oriented in north and one in south directions. The samples were collected weekly from July 1st, 2020 until September 2nd, 2020 at 08:00 each morning.

For each leaf sample, the fresh weight was first recorded, followed by a 24-hour immersion in a Petri dish filled with distilled water which was kept in darkness with a temperature of 5 ±1°C. After 24 hours, the leaves were removed, the surface water was blotted-off, and the turgid weight recorded. Samples were then oven-dried at 105 ± 1°C until a constant weight. Leaf RWC was calculated as shown in (1).

$$RWC\ (\%) = \frac{W - DW}{TW - DW} \times 100 \quad \textbf{(1)}$$

Here, *W* is the fresh weight of the leaf, *TW* is the turgid weight of the leaf, and *DW* is the dry weight of the leaf.

The collected leaves were also subjected to the field and lab measurements for eco-physiological parameters such us chlorophyll content and Nitrogen Balance Index (Figure 3) by means of a Dualex® Scientific Polyphenols and Chlorophyll Meter (FORCE-A, Orsay, France).

Figure 3 - Field (left) and lab (right) eco-physiological measurements of leaves used for relative water content (RWC) analysis.

2.4.2 Disease

Disease data was collected on five separate days, July 2nd, July 21st, August 3rd, August 10th, and August 24th. On each collection date, 50 leaves from each of the 20 trees were chosen randomly and taken to the lab in order to measure the percentage of NLA. Here, an image analysis software (ImageJ [2]) was utilized in order to determine the percentage of NLA. The mean value across the 50 leaves was then taken as the representative value for each tree. Trees were also visually inspected for the occurrence of other diseases, such as bark cancers or root rots, but no symptoms were observed.

2.5 Internet of Things (IoT) data

To provide supplementary measurements, a weather station (Terrasense Vantage Pro2) has been installed next to the experimental site. Figure 4 illustrates the rainfall data collected over the course of 2020. Within the time frame of our water stress experiments we witnessed a large period of drought. However, the month of June, as well as earlier months, had large amounts of rainfall, leading to moist soil conditions during the summer season.

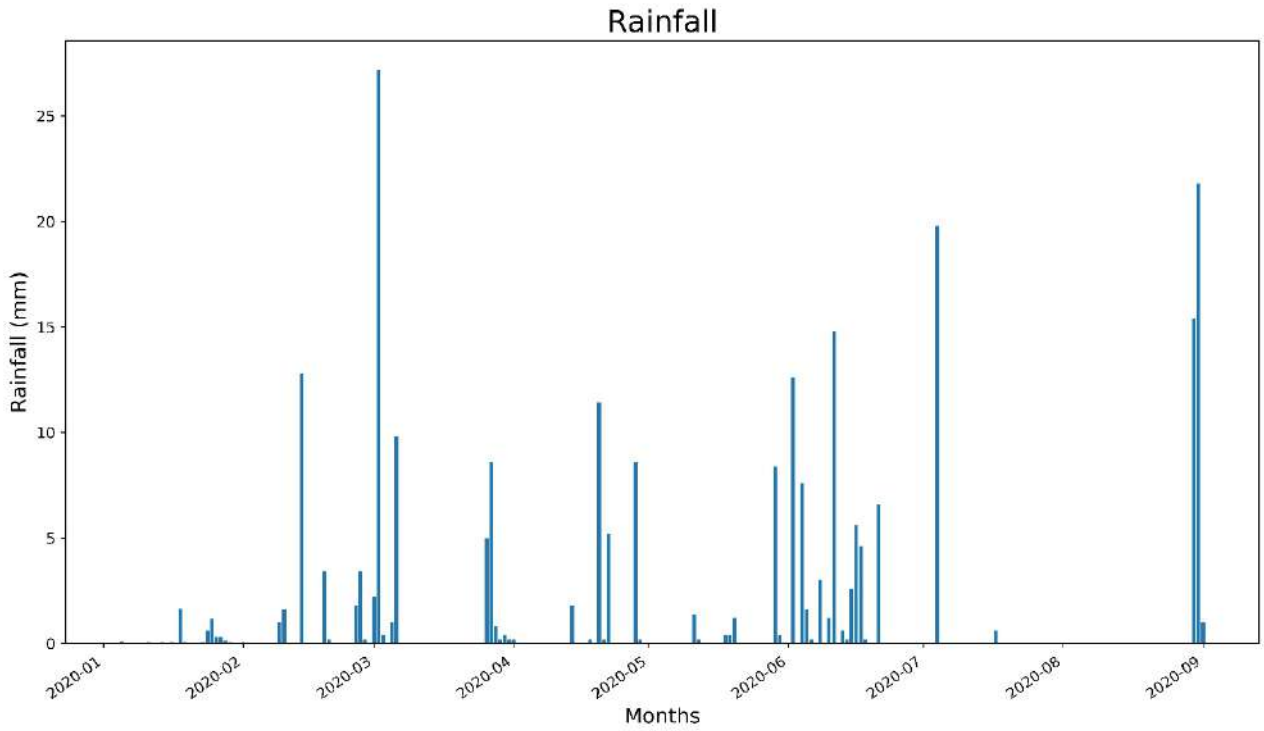

Figure 4 – Amount of rainfall (per day) over the course of 2020.

3 Data pre-processing

3.1 Quality check

Over the course of the data collection season, data quality checks were performed for each new UAV campaign in order to quantify the amount of blurry, over-, and under-exposed images for each sensor in each flight campaign, as well as to identify any possible sensor or GPS failures in a timely manner.

GPS positions were extracted with the use of the D-RTK from DJI. Due to the configuration of the UAV, GPS information was initially available for the Tetracam MCAW-6 images. However, a script tasked with the proper naming of files allowed us to match images taken by the Sony a5100 sensor with the GPS positions of the Tetracam based on the timestamps. Because the TeAx ThermalCapture has no internal clock, this was not possible and thus no GPS coordinates were available for these images. Although GPS coordinates were available, the automatic georeferencing performed by Metashape was inconsistent and often resulted in poorly georeferenced orthomosaics. As such, all orthomosaics were georeferenced manually to ensure proper alignment with tree coordinates.

Given the situation with COVID-19, we were unable to calibrate the exposure time of the Tetracam MCAW-6 in the field. As such, a look-up table was developed in order to choose a fixed exposure time based on readings from the on-site solar radiation station. Unfortunately, the look-up table resulted in certain bands being heavily underexposed and after failed attempts to fine-tune the table, it was decided to fly with automatic exposure in order to avoid further issues of under/over-exposure. However, the use of automatic exposure was also problematic, as it led to large differences in vegetation pixel values due to changing rates of exposure time between the young and adult fields. This issue led to an inability to perform a robust empirical line correction for the Tetracam MCAW-6 imagery, and thus pixel digital numbers (DNs) were used rather than

reflectance values. The reasoning for this is that the empirical line correction performs a transformation from pixel values to reflectance values. However, the relationship between the pixel and reflectance values is only valid for images which share the same exposure time as the image used to derive the empirical line model. Thus, the ability to properly calibrate a fixed exposure setting before each flight is imperative for all future campaigns.

3.2 UAV pre-processing

3.2.1 Tetracam MCAW-6

Images were exported from the camera in 16-bit TIF format and converted to single band files. Image bands were then aligned according to band-wise derived homography matrices from which spectral indices were calculated.

Indices used in this deliverable in order to detect water stress from the Tetracam MCAW-6 are summarized in Table 2. In order to mitigate the effects of the differences in exposure time in the Tetracam, normalized indices, such as the NDVI and PRI, were preferred.

Index Name	Equation	Reference	Target
Simple Ratio Index	$SR = \frac{\rho_{NIR}}{\rho_{Red}}$	[3]	Chlorophyll content vegetation structure, foliage cover
Normalized Difference Vegetation Index	$NDVI = \frac{\rho_{NIR} - \rho_{Red}}{\rho_{NIR} + \rho_{Red}}$	[4]	Chlorophyll content, vegetation structure, biomass, LAI
Photochemical Reflectance Index	$PRI = \frac{\rho_{531} - \rho_{570}}{\rho_{531} + \rho_{570}}$	[5]	Stress-induced changes of chlorophyll/carotenoid ratio, light use efficiency, water stress

Table 2 - Vegetation indices calculated from the Tetracam MCAW-6 imagery for the detection of water stress and diseases.

3.2.2 TeAx ThermalCapture-2.0

Given that the thermal sensor of the Teax ThermalCapture-2.0 records videos rather than producing individual images, short videos are stored by the camera. During pre-processing, the first frame of each video is extracted and converted to a TIF file. The DNs of the thermal images are converted to apparent canopy temperatures (T) by applying Equation 2:

$$T = DN * 0.04 - 273.15 \quad \textbf{(2)}$$

After converting the DNs to temperature values, the Crop Water Stress Index (CWSI) (Equation 3) was calculated.

$$CWSI = \frac{T_s - T_w}{T_d - T_w} \quad \textbf{(3)}$$

Here, T_s is the temperature of the canopy, T_w is the lower boundary of the plant surface temperature, and T_d is the upper boundary of the plant surface temperature. Following the methodology of [6], we calculated T_w using the coolest 5% of the irrigated pixels, while T_d was estimated by adding 10 degrees to the air temperature at the time of flight. Air temperature was taken from the IoT network which takes readings once every 5 minutes.

3.3 Orthomosaic generation

Individual orthomosaics were generated from each flight for each of the three sensors (Fig. A 1, Fig. A 2, Fig. A 3). Orthomosaics were generated using Agisoft Metashape [7] and the same workflow as was presented in section 4.2.4 of *D4.5 – Pest and Disease Detection* was applied. For a more detailed discussion on the orthomosaic process we also refer the reader to *D4.3 – Aerial Image Processing Pipeline*.

Date	Comments	Effects
2020/07/12	• Full coverage (MCAW and TeAx). • Many missing images for the Sony due to a bug in the drone software update received by the integration company that was not yet detected.	• Missing Sony images had minimal effect as the TeAx and MCAW sensors were the focus of this deliverable.
2020/07/18	• Full coverage (MCAW and TeAx). • Many missing images for the Sony due to a bug in the drone software update received by the integration company that was not yet detected.	• Missing Sony images had minimal effect as the TeAx and MCAW sensors were the focus of this deliverable
2020/07/26	• TeAx and MCAW both missing the entire irrigated row on the adult side due to problems with the UAV system. The cause was identified and corrected for future flights. • Sony camera missing all images. • The cause of missing images from the Sony camera in previous flights was identified and corrected.	• Effect of the missing row in TeAx and MCAW was mitigated by examining only trees where both sensors overlapped • Missing Sony images had no effect on resulting analysis given the focus on TeAx and MCAW

2020/08/02	• A change in status of a nearby airfield forced us to lower the flight altitude. In an attempt to still cover the entire area in each flight, the speed of flight was increased, leading to problems with UAV triggering and resulting in a loss of images in the first flight. • Flights after this date were split in two to only cover a single field per flight to avoid problems caused by faster flight speeds.	• The second flight covered all but a few of the southern trees, as such the loss of data from the first flight was largely mitigated by the redundancy in our data collection
2020/08/08	• Only young side covered due to unknown UAV system failure during first flight on adult side.	• Could only analyze the young side on this date
2020/08/23	• Given the plan to fly 8 times on this day, we decided to fly only the bottom half of both fields 16 and 18 in order to capture a portion of each treatment group. • Increasing wind speeds and clouds led to less than ideal flight conditions as the day progressed	• Poor flight conditions led to loss in quality for some flights, but the data redundancy mostly made up for these losses
2020/08/29	• Full coverage for both MCAW and Sony. • No TeAx orthomosaic due to problems with image alignment in Metashape. • Presence of dark stripes indicate partial cloud coverage during the flight.	• Loss of TeAx meant this date could not be used as no overlap between MCAW and TeAx could be established
2020/09/05	• Sony missing all adult trees due to large holes caused by the inability of Metashape to find robust feature points. • Two trees missing from the adult field in both MCAW and TeAx.	• Quality of the Sony orthomosaic had little effect as the focus was the TeAx and MCAW sensors
2020/09/13	• Full coverage on both sides. • Some adult trees not well reconstructed by the software in the TeAx orthomosaic. • Presence of dark stripes indicate partial cloud coverage during the flight.	• Incomplete canopies could still be included in our analysis
2020/09/20	• Full coverage for Sony • Missing trees in both TeAx and MCAW due to problems with the reconstruction by the software. • Presence of dark stripes indicate partial cloud coverage during the flight.	• Could only use trees covered by both MCAW and TeAx in our analysis

Table 3 - Presents a summary of the flights from this season.

3.4 Feature extraction

In order to extract spectral features for each tree across all four indices we stacked the four index orthomosaics on top of each other and resampled them to an equal pixel size of 0.1m. Given that certain campaigns had only data from one of the two sensors we chose only campaigns where both the Tetracam MCAW-6 and the TeAx ThermalCapture 2.0 covered the same trees, resulting in 19 (out of 24) useable flights.

Features were extracted from the stacked orthomosaics by taking a 1.5m radial buffer around the center coordinate of each of the 20 trees. Given the 1.5m buffer size, some ground pixels were unintentionally extracted. In order to remove any possible ground pixels, we made use of the digital elevation models (DEMs) which are available as a byproduct when generating orthomosaics with Metashape. Thus, we selected only those pixels which corresponded to the upper 70th percentile of DEM values within the buffer zone. This ensured that only pixels which represent the crown of the canopy were selected for further analysis.

We utilized the same processing chain as mentioned in section 4.4 of *D4.5 – Pest and Disease Detection* in order to integrate extracted spectral features with ground truth measurements. Thus, the UAV dates were assigned to the closest temporal ground truth measurements.

4 Results

4.1 Influence of irrigation scheme and overall variability of leaf water content

In order to produce spatial variability of water availability, and therefore artificially induce and amplify the effects of water scarcity, a differential irrigation scheme was applied on the field (see also section 2.1). As a whole, 2020 was not particularly lacking in precipitation. However, there was a longer period devoid of rainfall during August (Figure 4), in which we hoped to see differences in the phenology between the irrigated on non-irrigated groups.

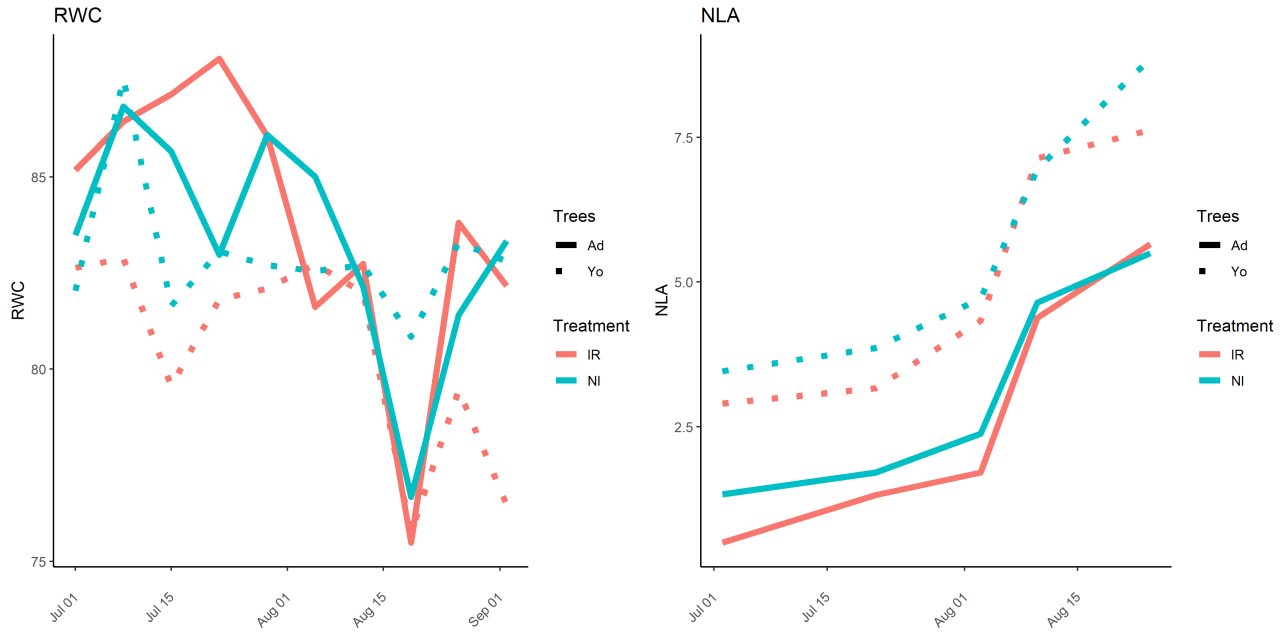

Figure 5 - Shows the development of the relative water content and necrotic leaf area for both the irrigated (blue) and non-irrigated (red) treatment groups. Adult trees are shown using solid lines while young trees are shown with the dotted line.

Even though no water stress occurred, we still have a decline in leaf water content in that period, but both observed parameters of the acquired ground truth dataset show relatively similar values for the two groups. Subsequent nonparametric significance tests for each observed date showed no consistent differences between the groups. Plant yields, as shown by nut production weight in kg per tree (see Figure 6), show some significant differences in the adult plants, but not in the young plants. Overall, the variability of both RWC and NLA is very low within each date, which makes establishing a relationship between UAV-acquired data and these ground truth measurements very difficult.

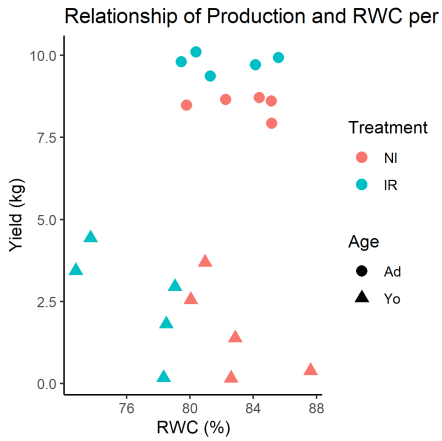

Figure 6 - Shows the distribution of relative water content and nut production by treatment and age

The main explanation for this phenomenon is based on the soil present in the study fields. The region of Viterbo contains excellent soil conditions for hazelnut trees, as the roughly 20,000 ha area requires that only about 25% of trees be irrigated. This has been supported by a soil texture analysis experiment which was carried out in 2019 by the University of Tuscia (UNITUS) following the methodology of [8]. Here, the available water content, expressed as mm of available water for plants per meter depth of soil, was calculated [9] at two points within field 18 and two points within field 16. The result of this analysis found that the soils from each field were highly homogeneous and characterized by a high capacity for water retention. Thus, given the combination of the rainy conditions earlier in the year with the water retention properties of the soil, we were unable to see sufficient variations between the RWC of the irrigated and non-irrigated fields.

4.2 Development of necrotic leaf area

Given that it is not conceivable to artificially inoculate fungal or bacterial pathogens in open field, the surveys were aimed to the measure of naturally occurring diseases. The necrotic leaf area (NLA) was assessed, as for the previous seasons, as a measure of the relevance of the main foliar disease of hazelnut, the leaf anthracnosis by *Piggotia coryli*. However, in 2020, the overall incidence of the disease was lower than in 2019 likely as a consequence of climatic conditions unfavourable for the disease development during the spring. Indeed, low precipitations have occurred in both April and May, which might have reduced the spread of the pathogen. On the other hand, in the latest samplings of 2020 some of the leaves randomly collected on the tree canopies were found to be almost completely desiccated. These damages do not seem referable to the fungal disease, but more likely to abiotic causes, such as a sun burst, given the hot temperatures registered during the summer 2020. In support of this hypothesis, *Piggotia coryli* was isolated from (some) leaves showing the typical disease symptoms but not from representatives of desiccated leaves. Unfortunately, due to the huge number of leaves analysed (1000 per each collection date) it was not possible to verify this

hypothesis and discriminate the NLA referable to the fungal disease from that referable to the abiotic factors for the whole analysis.

4.3 Index maps

Figure 7, Figure 8 and Figure 9 show all indices for the 19 flight campaigns with equal coverage between the Tetracam MCAW-6 and the TeAx ThermalCapture 2.0. The raster plots highlight several problems with the data acquisition. Firstly, the coverage is spottier in the later dates, which shows that a flight altitude of 25 meters is not enough to cover the entire study area. Secondly, value ranges differ greatly from date to date, for reasons which are different for the optical and thermal sensors. One of the reasons is that the MCAW images require empirical line correction to be comparable, but this could not be conducted because of varying exposure settings. Another reason is that the CWSI values require theoretical minimum (wet) leaf values, which we had to compute empirically, based on the image. This is a problem, because the areas covered across the various orthomosaics are different, meaning that the empirical basis on which minimum canopy temperatures are computed also differs. As a consequence, CWSI values of different dates are not comparable. This is particularly obvious looking at the development of the tree values, illustrated in Figure 10, where it is very obvious that there are massive differences in value ranges between some of the dates, which are pure artifacts caused by problems in the datasets. We describe possible changes to improve dataset quality and consistency for next year, most importantly the change of altitude and calibration of the exposure lookup table, in section 5.3.

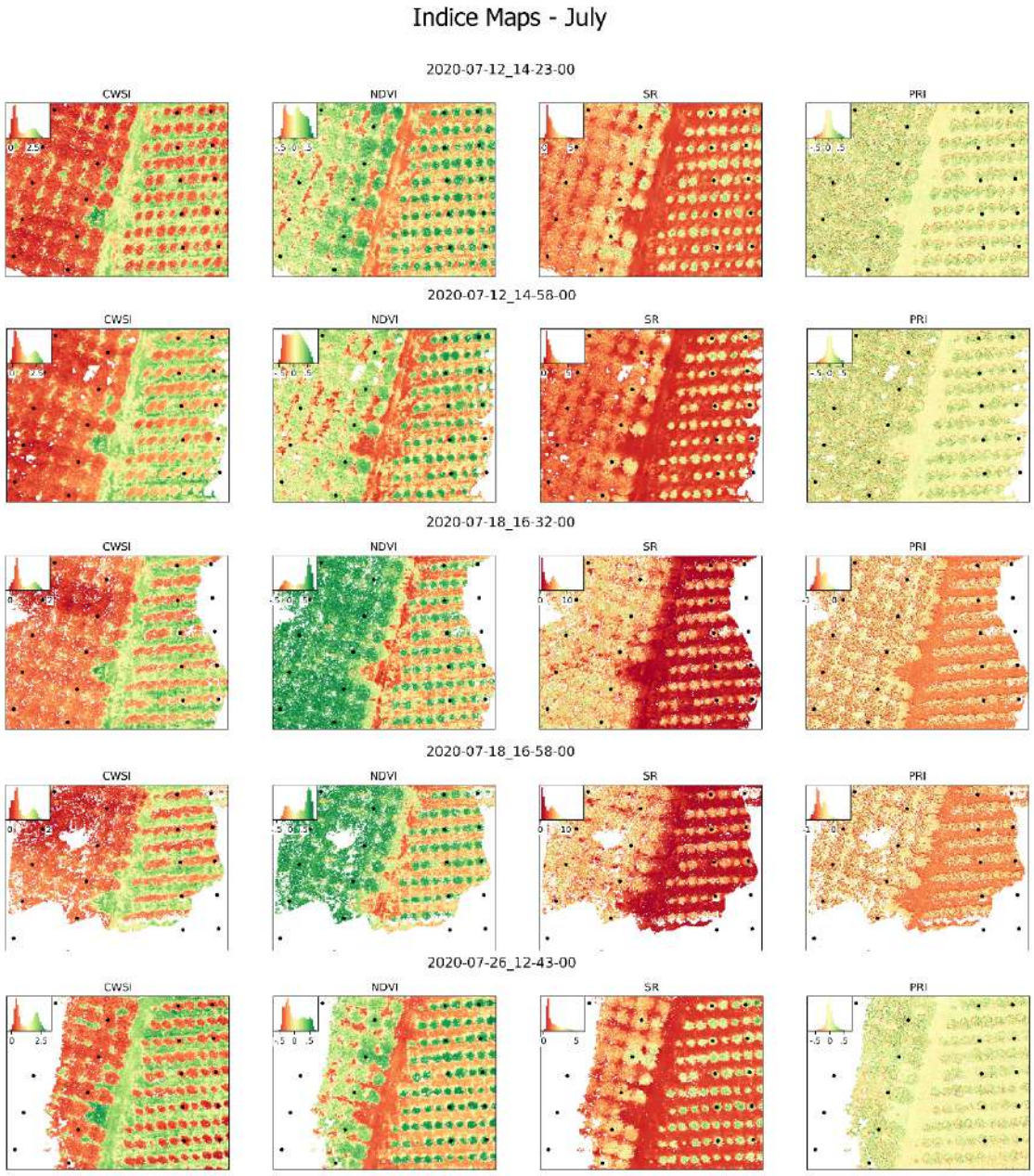

Figure 7 - Index maps for flight campaigns carried out in the month of July. Shows the Crop Water Stress Index (CWSI), Normalized Difference Vegetation Index (NDVI), Simple Ratio (SR), and Photochemical Ratio Index (PRI). Dates show the year, month, day, hour minute and seconds of each given flight campaign.

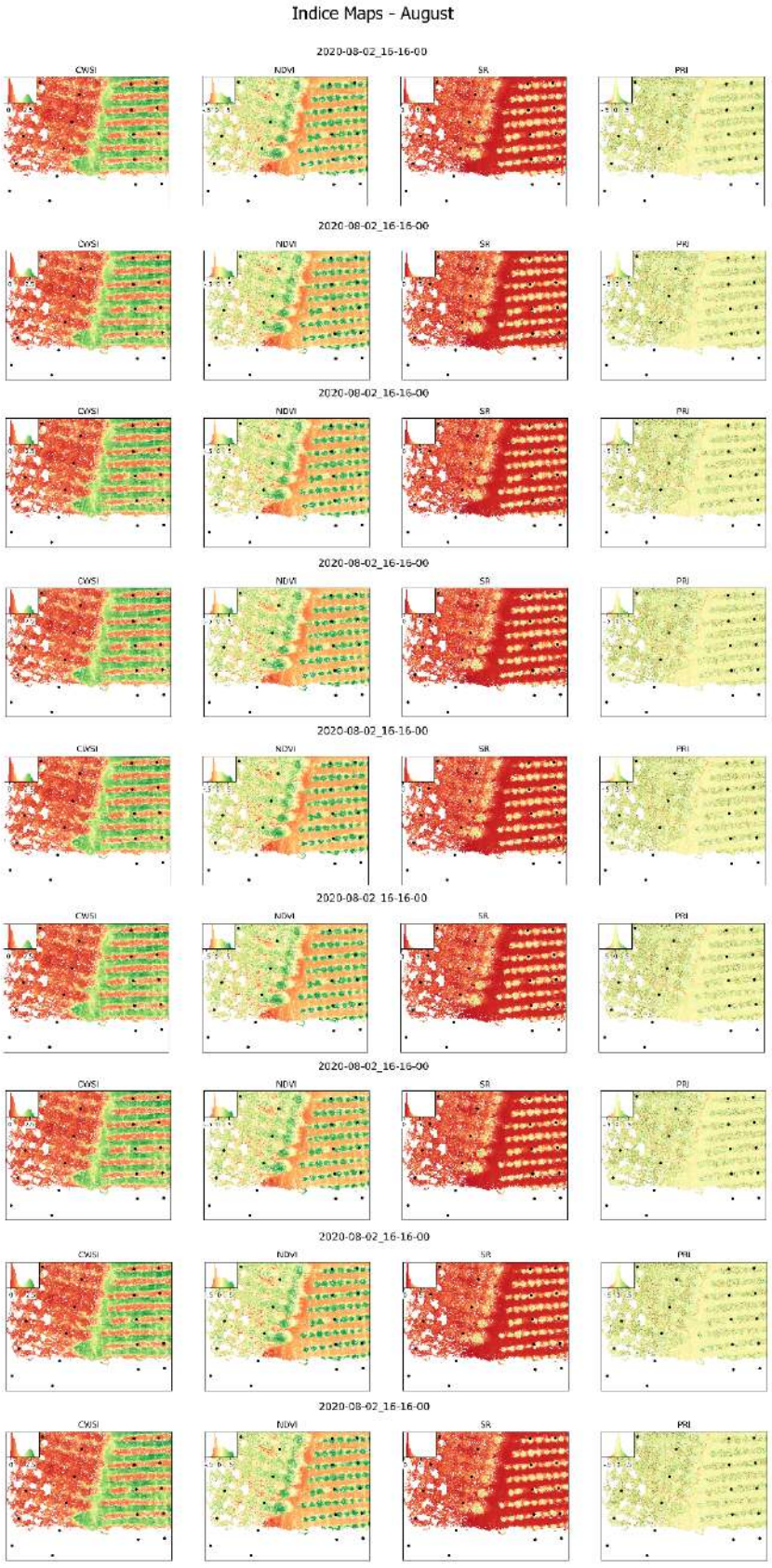

Figure 8 - Index maps for flight campaigns carried out in the month of August. Shows the Crop Water Stress Index (CWSI), Normalized Difference Vegetation Index (NDVI), Simple Ratio (SR), and Photochemical Reflectance Index (PRI). Dates show the year, month, day, hour minute and seconds of each given flight campaign.

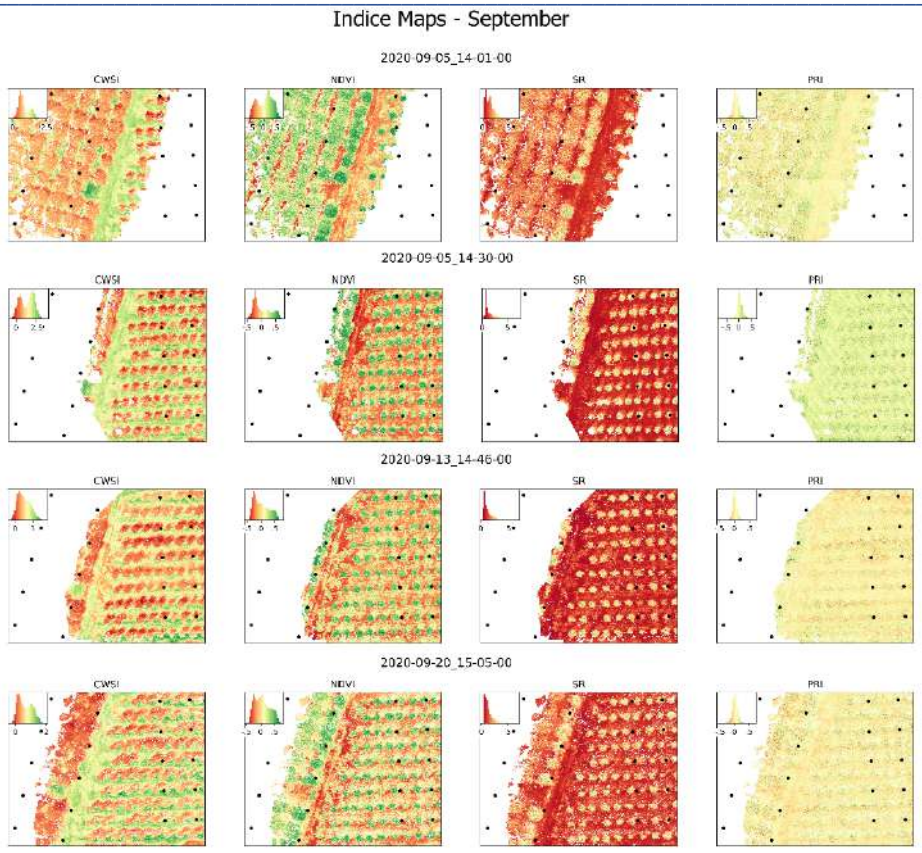

Figure 9 - Index maps for flight campaigns carried out in the month of September. Shows the Crop Water Stress Index (CWSI), Normalized Difference Vegetation Index (NDVI), Simple Ratio (SR), and Photochemical Reflectance Index (PRI). Dates show the year, month, day, hour minute and seconds of each given flight campaign.

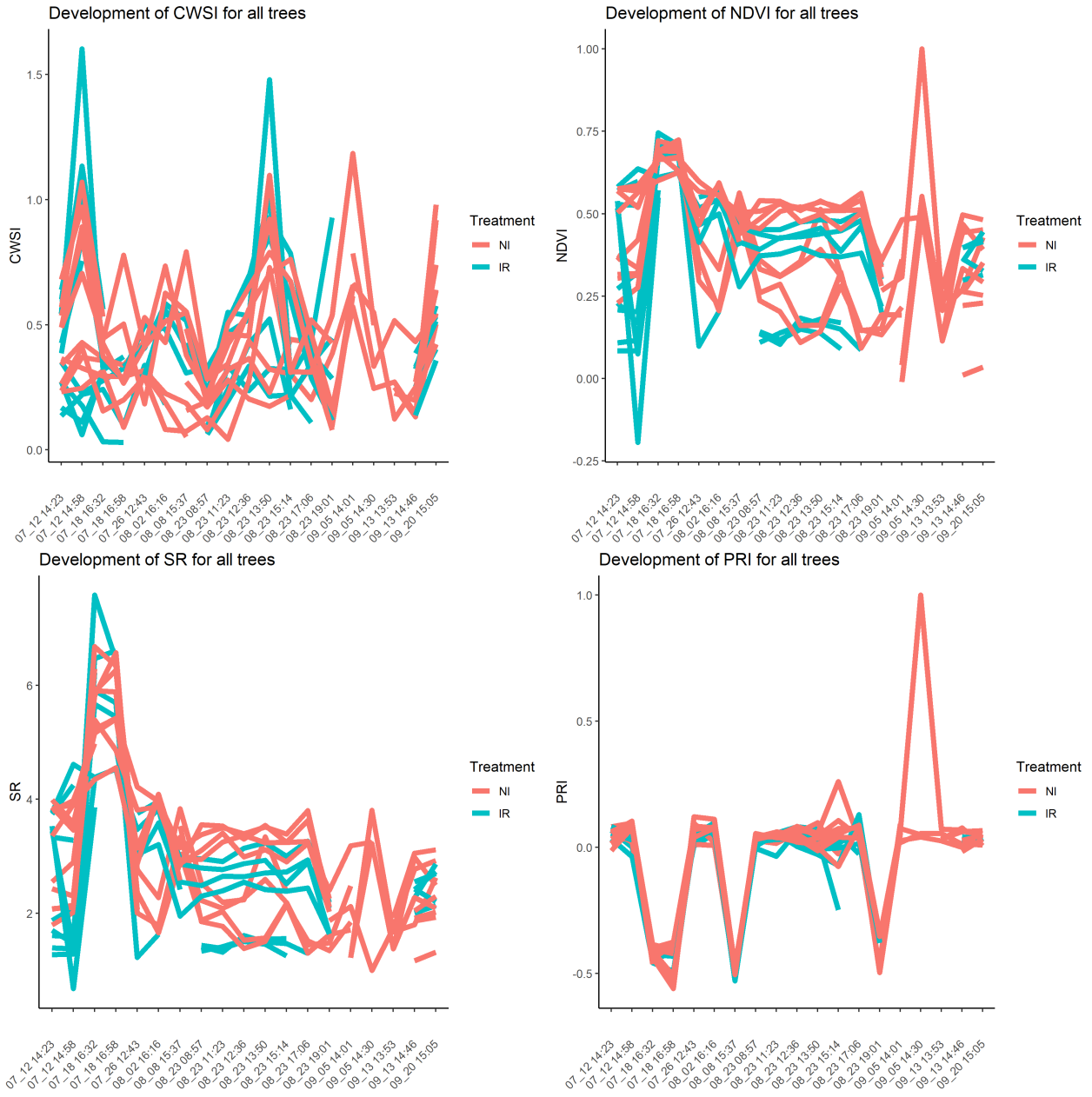

Figure 10 - Shows the development of each index over the course of the data collection season for both the irrigated (blue) and non-irrigated (red) treatment groups. Dates on the x-axis are formatted as "month_day hour:minute", indicating the time of flight for a given measurement. Breaks in the line indicate gaps in the data.

4.4 Correlation analysis

Based on the aforementioned differences in values ranges for different dates, modeling across different dates is next to impossible. Modeling within a given date works much better, but is also difficult as the overall variability on a single date is very low (see Figure 5). Nonetheless we tried to model the two phenology parameters based on the four indices with two different approaches. A univariate approach was used to measure the correlation between each index and each phenology parameter for each single date. Figure 11 shows scatter plots with regression lines for each flight campaign. While there is no clear trend in the combined dataset with all dates, modeling based on subsets for each individual date showed some promise,

with values that were highest for the dates with complete coverage. Measures to improve between date comparability for all indices will be outlined in section 5.3.

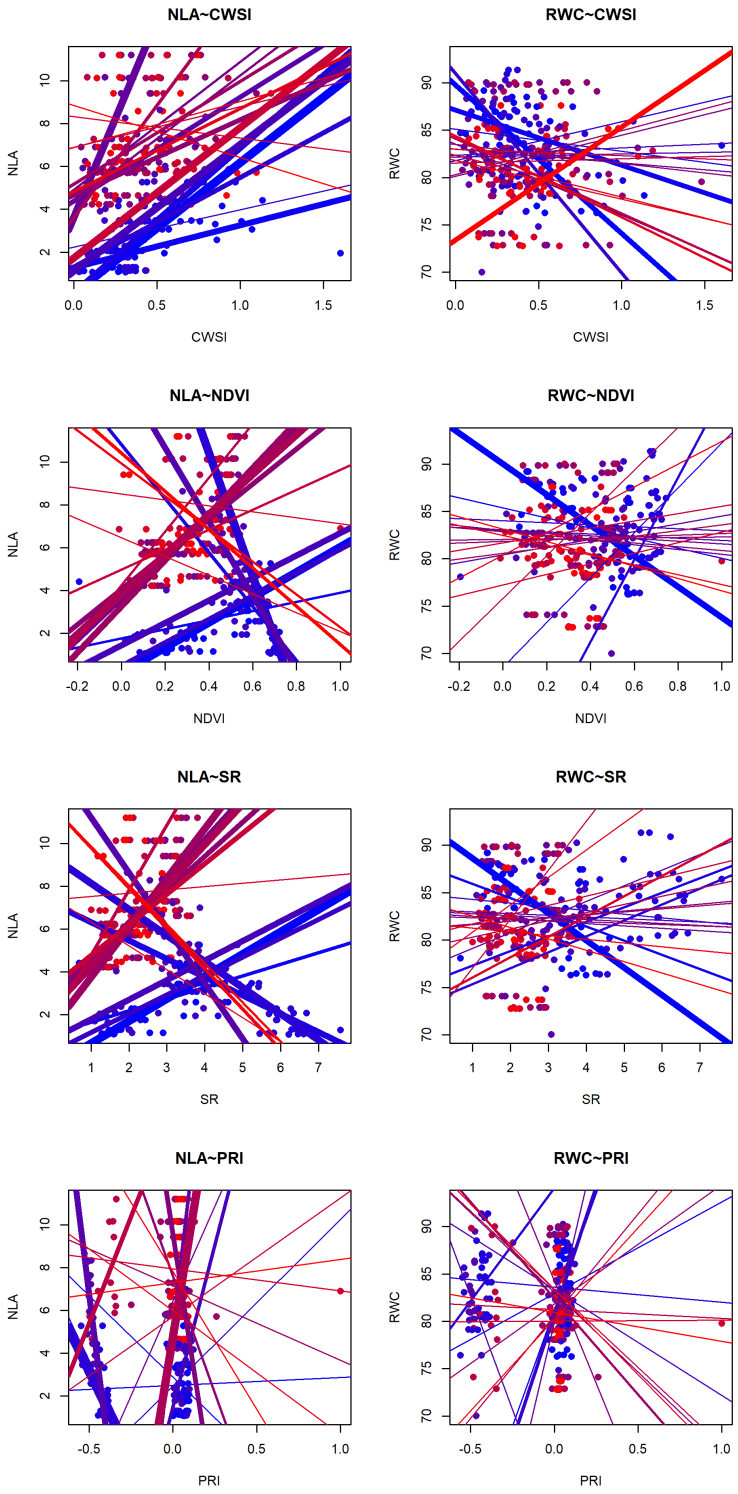

Figure 11 - Univariate model plots. Lines indicate the modelled relationship between the variables for a given flight, while points represent single tree measurements across all flights. Coloring indicates the date of the flight, with blue indicating earliest dates and red indicating later dates, while line thickness indicates the modeled R-squared value (thicker is higher).

All univariate model performances are also described in Table 4 and Table 5. The tables also show the second multivariate modeling approach, with which we tried to predict the phenology parameters based on all four indices.

Correlation NLA	CWSI	NDVI	SR	PRI	Multi
2020-07-12_14-23-00	0.63	0.65	0.66	0.02	0.7
2020-07-12_14-58-00	0.44	0.15	0.26	0	0.56
2020-07-18_16-32-00	0.43	0.26	0.4	0.08	0.56
2020-07-18_16-58-00	0.36	0.66	0.56	0.79	0.86
2020-07-26_12-43-00	0.02	0.38	0.38	0.05	0.44
2020-08-02_16-16-00	0.6	0.5	0.48	0.28	0.67
2020-08-08_15-37-00	0.35	0.48	0.5	0.42	0.75
2020-08-23_08-57-00	0.52	0.39	0.4	0.23	0.63
2020-08-23_11-23-00	0.19	0.51	0.53	0.07	0.53
2020-08-23_12-36-00	0.19	0.44	0.46	0.36	0.55
2020-08-23_13-50-00	0.4	0.38	0.37	0.15	0.5
2020-08-23_15-14-00	0.22	0.48	0.52	0.03	0.65
2020-08-23_17-06-00	0.25	0.58	0.58	0.64	0.84
2020-08-23_19-01-00	0.05	0.2	0.22	0.33	0.41
2020-09-05_14-01-00	0.52	0.2	0.32	0.01	0.56
2020-09-05_14-30-00	0	0.01	0	0.02	0.27
2020-09-13_13-53-00	0.27	0.05	0.04	0.03	0.44
2020-09-13_14-46-00	0.01	0.2	0.2	0.03	0.22
2020-09-20_15-05-00	0.06	0.24	0.16	0	0.43

Table 4 - Univariate model R2 values between necrotic leaf area (NLA) and vegetation indices. 'Multi' provides the R2 value derived from the multivariate model incorporating all four indices as independent variables.

Correlation RWC	CWSI	NDVI	SR	PRI	Multi
2020-07-12_14-23-00	0.36	0.43	0.43	0.09	0.47
2020-07-12_14-58-00	0.33	0.08	0.17	0.01	0.45
2020-07-18_16-32-00	0	0.09	0.13	0	0.22
2020-07-18_16-58-00	0.04	0.16	0.11	0.18	0.48
2020-07-26_12-43-00	0.26	0	0.01	0.22	0.64
2020-08-02_16-16-00	0	0.01	0.01	0.01	0.09
2020-08-08_15-37-00	0	0	0.03	0.04	0.32
2020-08-23_08-57-00	0.01	0	0	0.05	0.11
2020-08-23_11-23-00	0	0	0	0.01	0.02
2020-08-23_12-36-00	0.02	0	0	0.04	0.14
2020-08-23_13-50-00	0.02	0	0	0.01	0.1
2020-08-23_15-14-00	0.03	0	0	0.17	0.23
2020-08-23_17-06-00	0	0.01	0.02	0.02	0.19
2020-08-23_19-01-00	0.12	0.09	0.09	0	0.25
2020-09-05_14-01-00	0	0.05	0.05	0.04	0.28
2020-09-05_14-30-00	0.02	0.05	0.14	0	0.49
2020-09-13_13-53-00	0.18	0.05	0.04	0.04	0.24
2020-09-13_14-46-00	0.01	0.02	0	0.02	0.2
2020-09-20_15-05-00	0.4	0.03	0.02	0	0.49

Table 5 - Univariate model R2 values between relative water content (RWC) and vegetation indices. 'Multi' provides the R2 value derived from the multivariate model incorporating all four indices as independent variables.

Overall, it can be said that the within date correlation analysis worked much better than the across date correlation analysis, which showed no significant correlation between the indices and the phenology parameters. But as the correlation coefficients in Table 4 and Table 5 show, these relationships are still comparatively weak. Correlation coefficients are strongest, where lots of trees are present, especially in the two flights from the 12th of July, where all trees were covered. They are also stronger for the NLA which generally seems to correlate much better with the UAV data. Looking at the indices, the PRI seems to contain the least amount of information, since its correlation values are very low across most of the dates.

4.5 Drought stress risk maps

Overall, the multivariate regression shows the most promise, even though the data quality as well as the lack of drought stress in the field prohibit a more in-depth modeling analysis. Thusly, we tried to model the phenology variables for the given harmonized datasets of each date, in order to provide a quantified assessment of the current state of the field (Figure 12 and Figure 13). Overall, it can be said that the approach worked technically, but cannot be validated with the current available datasets because of issues mentioned in section 4.3. As soon as more complete datasets are available, more fitting modeling approaches need to be chosen in order to reflect the value distribution and nonlinearity of the regression problem.

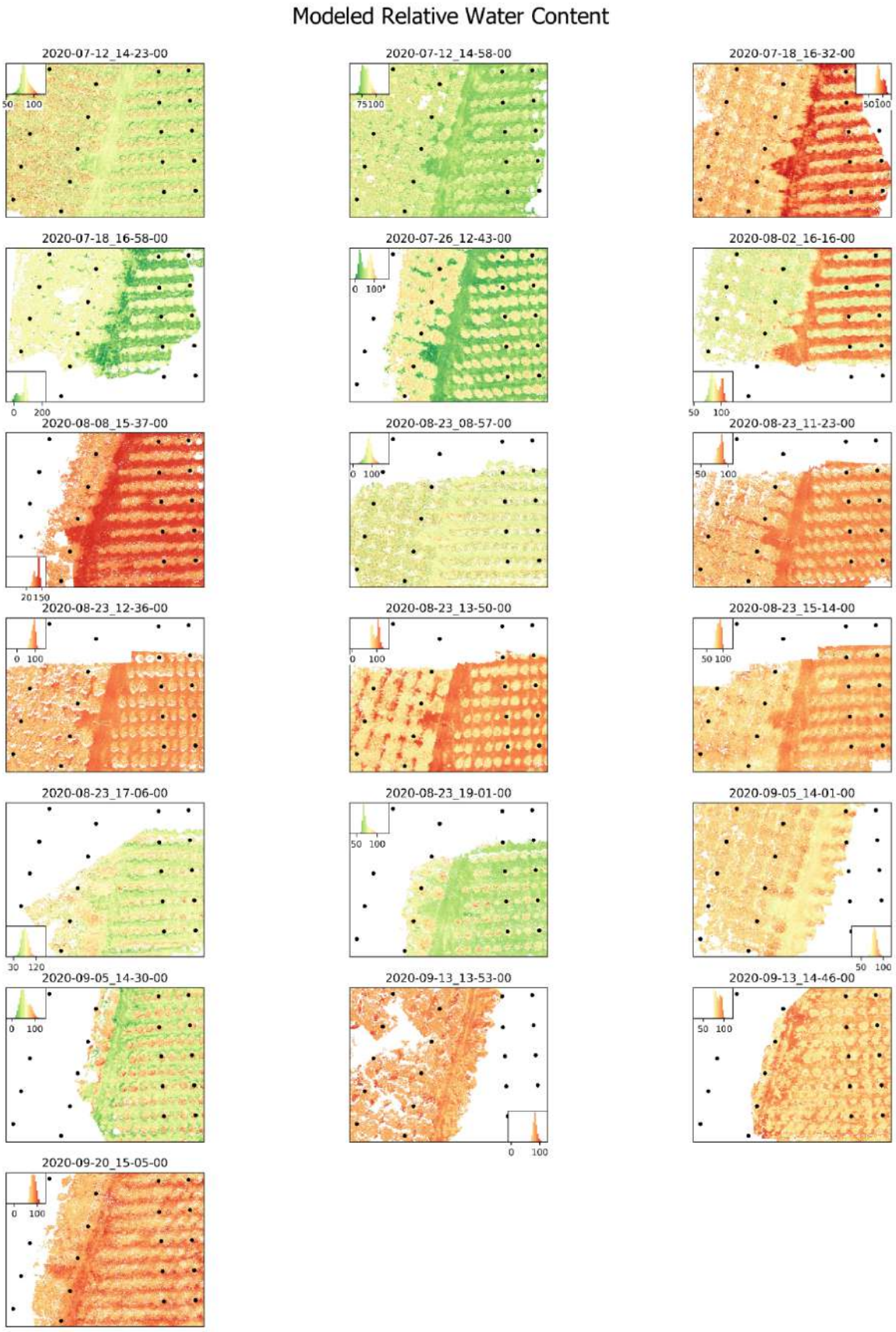

Figure 12 - Predicted relative water content values based on a multivariate regression, from low (green) to high (red).

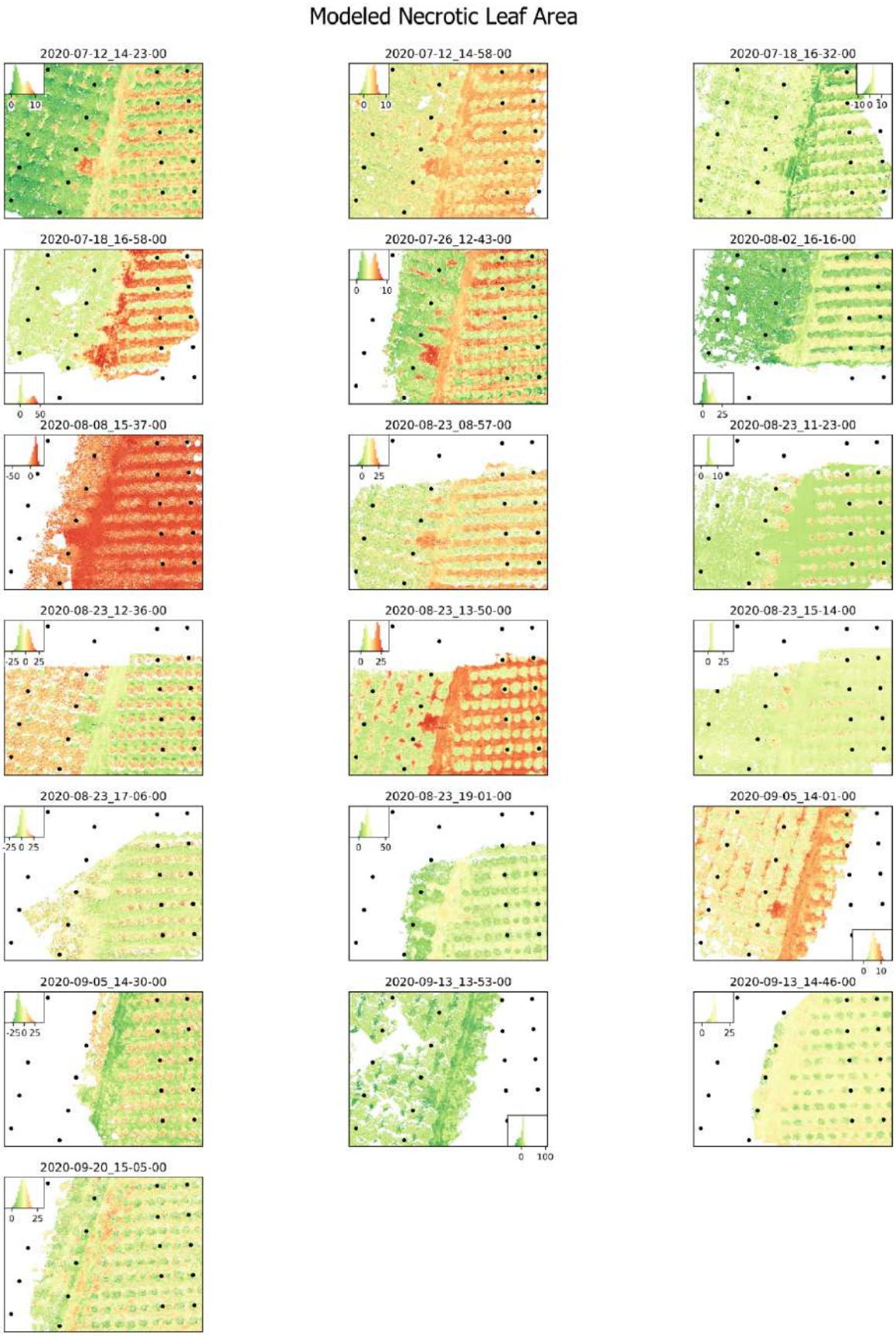

Figure 13 - Predicted necrotic leaf area values based on a multivariate regression, from low (green) to high (red).

5 Conclusions and comments

5.1 Task related criticalities

5.1.1 Phenology related issues

As elaborated in section 4.1, the measured phenology parameters were severely lacking in variability, which made our multivariate modelling and correlation analysis very difficult. Water availability of the plants was influenced by irrigation and precipitation. The precipitation, as described in section 2.5 was comparatively low in August, but overall, it was not a very dry year. The irrigation scheme itself was shown to have no significant influence on the leaf phenology.

5.1.2 Remote sensing related issues

5.1.2.1 Platform integration issues

The integration of all three sensors on the UAV platform was a topic of constant adjustment, but by the end of the season most issues were fixed. One big problem that we were unable to solve was the exposure lookup table, due to COVID-19 related travel restrictions.

5.1.2.2 Mission planning related issues

The complexity and the continuously changing nature of the current Italian aviation regulations revealed to be a major limiting factor during the 2020 data acquisition campaign. We believe it is important to highlight this fact as flight restrictions represented the main limiting factor for our data acquisition. We believe that clear and stable rules and mechanisms for an easier access to airspace for agricultural drones (which by definition fly in remote and in not inhabited areas) should be established by the legislator.

Due to these unforeseen restrictions, the UAV could only be operated at very low altitudes, and only on very specific days. This causes two major problems. Firstly, the image overlap is very low, which resulted in a much smaller footprint of the orthomosaic. Additionally, we observed large gaps in the imagery because the software was unable to find matching points because of the much bigger parallax effects. Secondly, since we do not have the choice of when to fly, suboptimal cloud conditions is often the only choice. Flying in 100% cloud free weather is crucial for optimal image results.

The resulting problems of very low flight altitude, as well as flying under potentially cloudy conditions also interact and exacerbate our platform integration issues. Even automated exposure settings would have been less consequential in higher altitude because the reflected light level would have been much more constant. Missing images would have had a lesser impact, because the overlap would have provided more redundancy.

5.2 Completed tasks

In order to mitigate the orthomosaicking issues, we largely adjusted our UAV preprocessing chain with the following measures:

- Converting raw images to indices before mosaicking to adjust for the varying exposure (MCAW)
- Manual georeferencing (Latitude and Longitude) of the orthomosaics due to problems with Metashape's automatic georeferencing
- Extracting canopy values based on local DEM maxima rather than a true ground/canopy segmentation

Based on these extracted values we developed multivariate modeling algorithms to predict on site phenology from remote sensing data. We then applied these models to the harmonized raster data for each date, and calculated maps that can be used to make spatially explicit assumptions about the situation on the field. In consequence of the points summarized in section 5.1, we mapped out a strategy to improve our data acquisition in 2021, laid out in section 5.3.

5.3 Further procedure

5.3.1 Fixing phenology related issues

Problems in observing real world drought stress was always a potential risk predicted in the proposal. Aside from hoping that we will be able to observe more severe effects in the upcoming year, there are potential other actions that could increase the variability of the measured variables on the field. We could increase the number of observed trees in order to have a higher population and therefore variety. To counteract the higher workload, we could decrease the number of observation dates. Additionally, we could schedule observations at different times during the day (8:00, 12:00, 16:00) in order to detect when plants show temporary daily phases of water stress. However, for this to make sense, we would require that UAV flights coincide with the times of these measurements.

5.3.2 Fixing remote sensing related issues

In view of the crucial data collection campaign of summer 2021, a series of actions have been planned, as well as some worst-case mitigation actions. After many attempts, we got in contact with the administration managing the Romeo area where we are flying, which gave us all the details on how to proceed with obtaining a derogation to both restrictions. If granted, this would allow us to fly an additional one or two days in the middle of the week and at higher altitude. Secondly, a week of preliminary tests with all the units involved will be carried out tentatively in beginning of March to finalize the sensor integration of the Tetracam MCAW-6.

Though it seems very likely that a way around the flight restrictions will be found for 2021, we also could do some adjustments to the sampled area. We could reduce the overall footprint of the orthomosaic and increase the density of sampled trees. This would probably result in less variability, but would stabilize the image overlap because we could fly slower.

Thought it is very much possible that travel restrictions will be lifted in spring 2021, it is far from certain. The exposure lookup table of the MCAW is mostly a logistical problem that requires an experimental setup on the field, and enough time to measure in varied solar conditions. If travel restrictions persist through winter, the experimental setup could be performed locally by the pilot, but with extensive instructions that could be developed by the University of Trier.

5.4 Summarized comments

We successfully developed an automated processing chain to monitor leaf water content in Hazelnut trees based on UAV imagery. Optical and thermal indices were used to predict spatially explicit phenological variables and produce detailed maps of the study site. Three major issues made validating our models impossible. Firstly, the flight regulations prevented us from proper data acquisition. It was too late to change this in 2020 but we will do our best to change it in 2021. Secondly, the sensor integration and calibration. We fixed most of the issues we had during the campaign and will fix the rest before the start of the season in

2021. Lastly, the lack of drought stress as a result of sufficient precipitation. We cannot influence precipitation, but we will further adjust the experimental design to allow for more variability.

6 References

[1] H. Barrs and P. Weatherley, "A Re-Examination of the Relative Turgidity Technique for Estimating Water Deficits in Leaves," *Aust. J. Biol. Sci.*, vol. 15, no. 3, p. 413, 1962.

[2] C. A. Schneider, W. S. Rasband, and K. W. Eliceiri, "NIH Image to ImageJ: 25 years of image analysis," *Nature Methods*, vol. 9, no. 7. NIH Public Access, pp. 671–675, Jul-2012.

[3] C. J. Tucker and P. J. Sellers, "Satellite remote sensing of primary production," *Int. J. Remote Sens.*, vol. 7, no. 11, pp. 1395–1416, 1986.

[4] J. W. Rouse, R. H. Haas, J. A. Schell, and D. W. Deering, "Monitoring vegetation systems in the Great Plains with ERTS." 1973.

[5] J. A. Gamon, L. Serrano, and J. S. Surfus, "The photochemical reflectance index: An optical indicator of photosynthetic radiation use efficiency across species, functional types, and nutrient levels," *Oecologia*, vol. 112, no. 4, pp. 492–501, Dec. 1997.

[6] M. Gerhards, G. Rock, M. Schlerf, and T. Udelhoven, "Water stress detection in potato plants using leaf temperature, emissivity, and reflectance," *Int. J. Appl. Earth Obs. Geoinf.*, vol. 53, pp. 27–39, Dec. 2016.

[7] L. Agisoft, "Agisoft Metashape Professional Edition." Petersburg, 2019.

[8] J. Tardaguila, M. P. Diago, S. Priori, and M. Oliveira, "Mapping and managing vineyard homogeneous zones through proximal geoelectrical sensing," *Arch. Agron. Soil Sci.*, vol. 64, no. 3, pp. 409–418, Feb. 2018.

[9] K. E. Saxton and W. J. Rawls, "Soil Water Characteristic Estimates by Texture and Organic Matter for Hydrologic Solutions," *Soil Sci. Soc. Am. J.*, vol. 70, no. 5, pp. 1569–1578, Sep. 2006.

7 Appendix

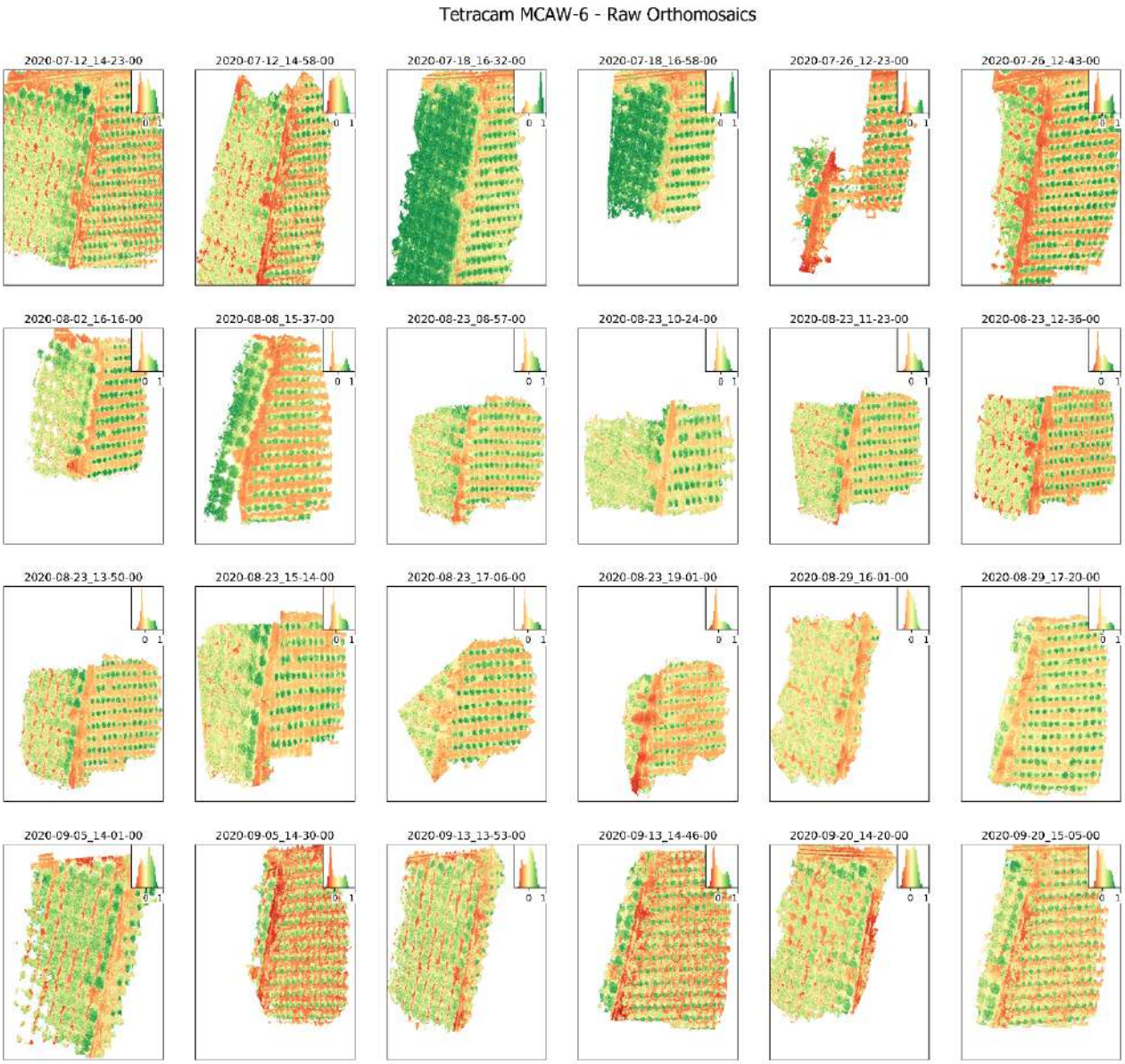

Fig. A 1 - Shows all orthomosaics produced from the Tetracam MCAW-6 in the 2020 data collection season. Pixel values are normalized difference vegetation index values ranging from -1 to 1.

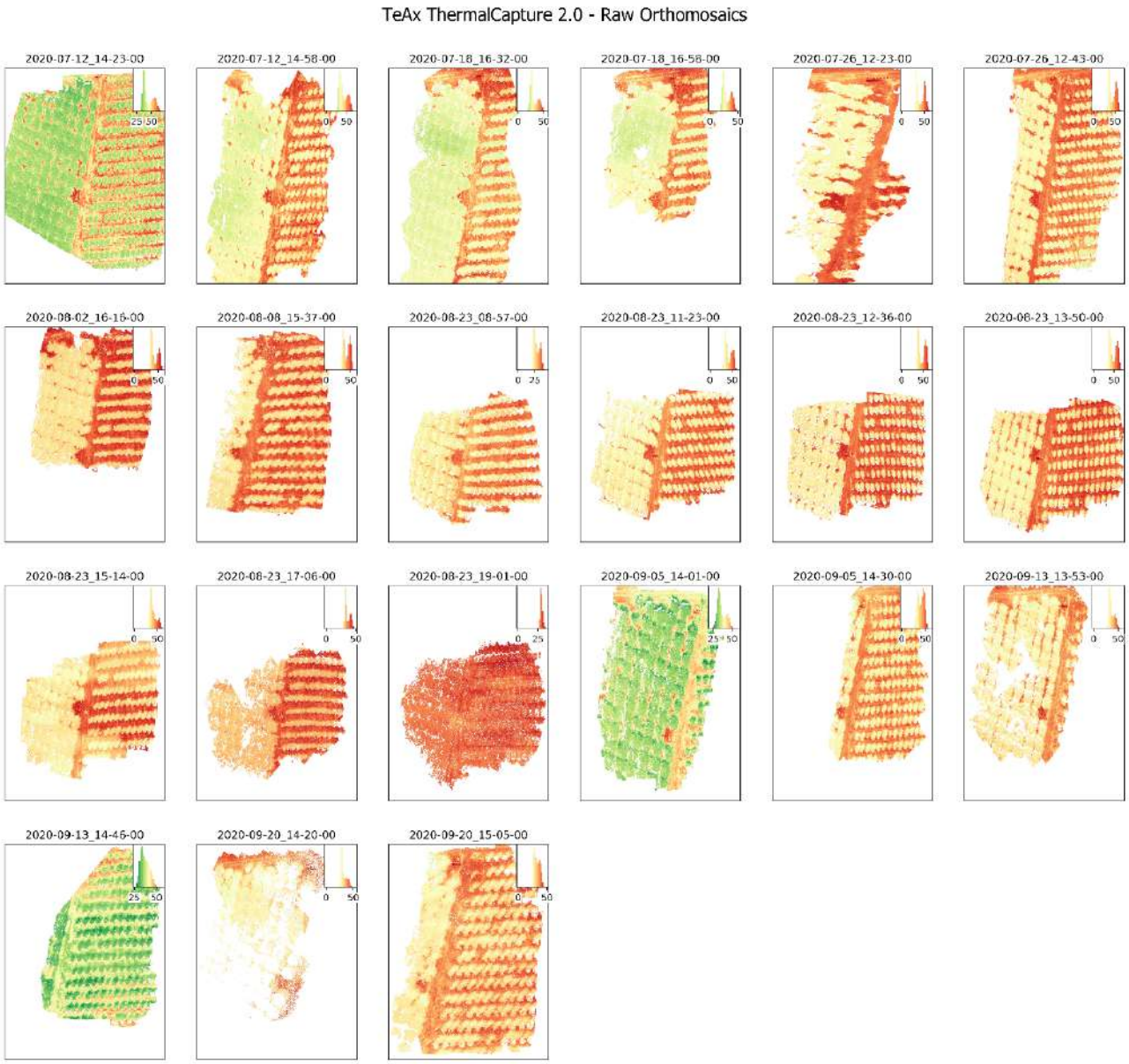

Fig. A 2 - Shows all orthomosaics produced from the TeAx ThermalCapture 2.0 in the 2020 data collection season. Pixel values are raw temperature values.

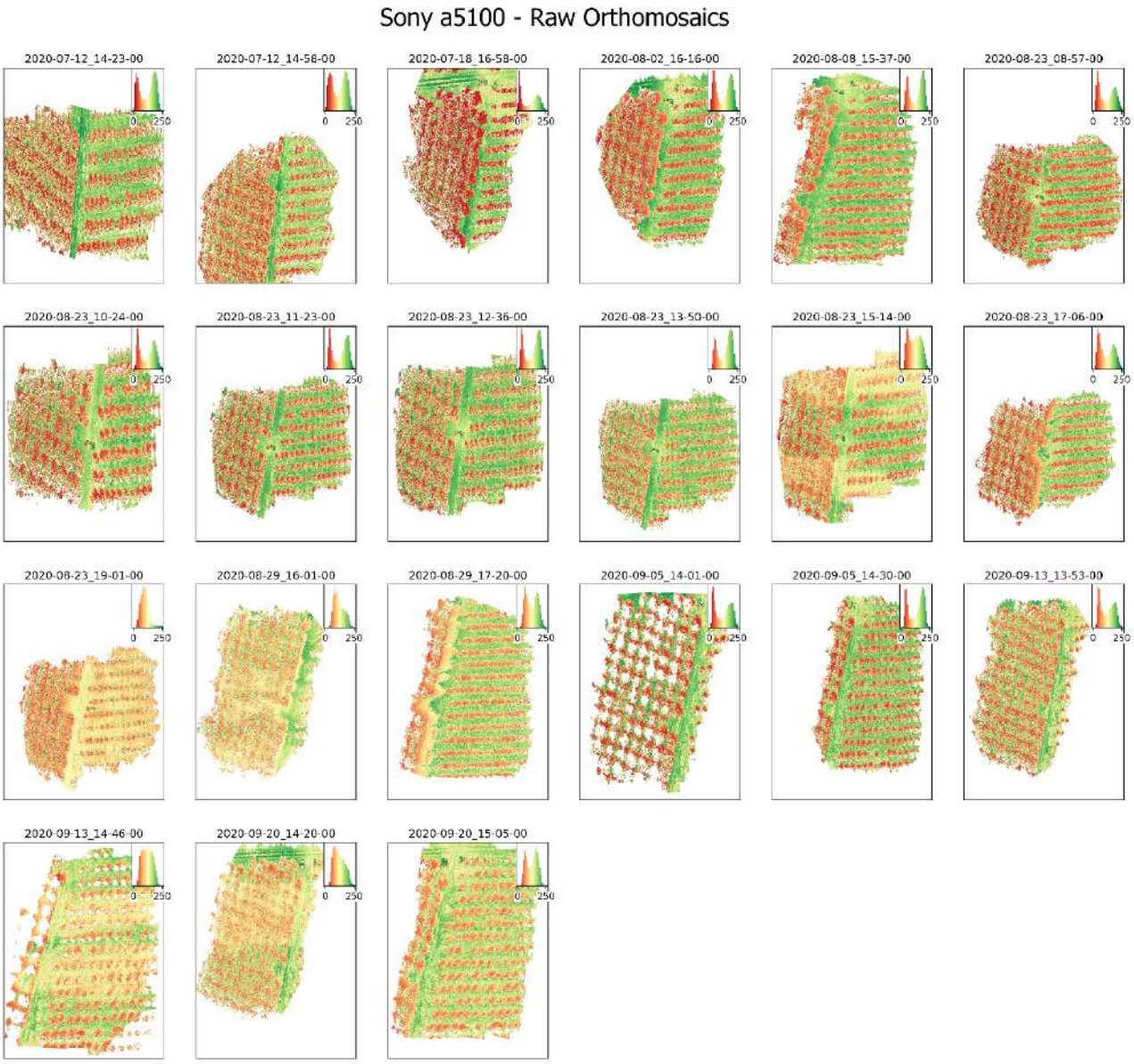

Fig. A 3 - Shows all orthomosaics produced from the Sony a5100 in the 2020 data collection season. Pixel values are raw digital numbers (Band 1).